Diagnosing Climate Change and Ocean Ventilation Using Hydrographic Data

NATHANIEL L. BINDOFF* AND TREVOR J. McDOUGALL*,†

*Antarctic Co-operative Research Centre, University of Tasmania, Hobart, Tasmania, Australia
†CSIRO Division of Oceanography, Hobart, Tasmania, Australia

(Manuscript received 30 December 1992, in final form 23 June 1993)

ABSTRACT

Changes in atmospheric forcing can affect the subsurface water column of the ocean by three different mechanisms. First, warmed mixed-layer water that is subducted into the ocean interior will cause subsurface warming; second, the subducted surface water can be freshened through changes in evaporation and precipitation; and third, the properties at a given depth may be changed by the vertical displacement of isotherms and isohalines without changes of water masses. These vertical displacements of the water column can be caused either by changes in the rates of renewal of water masses or by dynamical changes (such as changes in wind stress). A method for analysing the subsurface temporal changes in hydrographic data is described in terms of these three processes: "pure warming," "pure freshening," and "pure heave." Linear relations are derived for the relative strength of each process in terms of the observed changes of potential temperature and salinity in two different coordinate frames: (i) constant density surfaces, and (ii) isobaric surfaces.

Inverse methods are applied to three realizations of the SCORPIO section at 43°S in the Tasman Sea. These sections were obtained in 1967, and in the austral winter and summer of 1989 and 1990, respectively. This data is used to explore the relative strengths of surface warming, surface freshening, and heave of the water column. The six-month differences for this region show small changes in Sub-Antarctic mode water (SAMW) and are not characterized by any one process, whereas below the mode waters the observed differences are well described by the heave process. In contrast, the 23-year differences show significant changes in the properties of the water that flows into the Tasman Sea: SAMW (300–700 db) is well described by pure warming of near-surface waters, while the changes observed at the depth of the salinity minimum are consistent with pure freshening.

The observed changes in the interior of the ocean between adjacent seasons do not exhibit significant changes of water masses, consistent with the distance of this section from the outcrop region of the density surfaces of interest. For the 23-year differences, changed surface waters subducted into the ocean interior have sufficient time to influence the temperature–salinity correlations. The skill of our approach in discriminating between short-term changes (almost exclusively heave) and long-term changes associated with the subduction of changed surface waters is particularly encouraging. Although the observed changes could equally well be natural variability, they are qualitatively consistent with coupled numerical models of climate change in which surface waters are warmed and increased precipitation occurs south of the Sub-Antarctic Front.

1. Introduction

There are many ways in which changes in the coupled ocean–atmosphere system brought about by climate change may affect the oceanic thermocline. The most obvious change in the thermocline is likely to occur simply as a result of the subduction into the thermocline of warmed water from the mixed layer. Church et al. (1991) considered the warming of the ocean mixed layer and subduction of this warmed water along isopycnals (or neutral surfaces). A result of their work was that the subduction of warmed mixed-layer waters leads to a cooling and freshening of the subsurface thermocline water masses, when measured along isopycnal surfaces.

Corresponding author address: Dr. Nathan L. Bindoff, Antarctic Co-operative Research Centre, University of Tasmania, GPO Box 252C, Hobart, Tasmania, Australia 7001.

The subduction of warmed mixed-layer waters into the thermocline is just one result of climate change. Another result, found in coupled ocean–atmosphere models of the doubling of atmospheric CO_2 concentration (Manabe et al. 1990, 1991), is a decrease in sea surface salinity due to different spatial patterns of evaporation and precipitation. In addition to salinity changes, the winds (and their curls) are also likely to change significantly, causing the ocean gyres to change their structure.

The process of oceanic subduction where fluid from the mixed layer is incorporated into the thermocline for a steady ocean has been the subject of considerable research. On the basis of the similarity between the S–θ curve of the winter mixed layers at high latitudes and the vertical S–θ curve of casts in the central water thermocline, Iselin (1939) proposed that the water in the main thermocline was formed at the surface in late winter and subsequently moved downward and equa-

torward. Stommel (1979) examined the connection between the ocean mixed layer and the geostrophic flow below, and showed that the convergent Ekman layer pumped water down into deep geostrophic flow along isopycnal surfaces. Woods (1985) pointed out that in addition to the Ekman pumping, subduction occurs where the maximum depth of the winter mixed layer decreases in the direction of motion. This idea has been refined by Pedlosky and Robbins (1991) and Nurser and Marshall (1991) to include the distinction between Ekman pumping and the vertical velocity at the base of the mixed layer.

These ventilated thermocline theories have been used to explore the subduction of water in terms of a steady circulation. In this paper we explore the possible response of the ocean to three different changes in surface forcing as described above. Observations in the North Atlantic have shown significant changes have occurred in the salinity on isopycnals. Pollard and Pu (1985) interpreted these observations of freshening on isopycnals as resulting from changes in the patterns of surface precipitation in the North Atlantic. In contrast, Bindoff and Church (1992) found a freshening on isopycnals together with a warming of the main thermocline waters. They interpreted these observations as a warming of surface waters from a region of the Southern Ocean associated with Sub-Antarctic mode water. Here we show that in order to be able to distinguish between these quite different interpretations (surface freshening vs surface warming) of the same observed signal, one needs to view the changes of the salinity and potential temperature in both the isopycnal and in the geopotential coordinate frames.

In this paper we consider the effect of changes (i) in the temperature of surface waters, (ii) in sea surface salinity, and (iii) in the strength of the winds on subsurface hydrographic observations. These three processes have different signatures in potential temperature and salinity fields at constant depth and on neutral surfaces. The different signatures are used to estimate the relative strengths of each process for distinct neutral density classes for hydrographic data along the SCORPIO section at 43°S reported in Bindoff and Church (1992).

2. The three ventilation processes

In a steady-state ocean there is flow into a given density layer at some locations and outflow from the same density layer at other locations. Dianeutral advection of water across neutral surfaces also plays a role in the conservation of volume between two neutral surfaces. Global and regional warming will increase the flux of heat from the atmosphere into the ocean, and through air–sea interaction cause changes in the rates of evaporation and precipitation. In addition, the wind stress is also likely to change, thus altering the circulation and the depths of neutral surfaces. The effects of change in each of these three surface boundary conditions are considered here, one at a time. We initially concentrate on that part of the water column where the ratio $R_\rho = \alpha\theta_z/\beta S_z > 1$, typical of the main thermocline.

a. Pure warming

The first case we consider is due to the increase of heat flux across the sea surface, assuming the rate of evaporation minus precipitation to be unchanged. The physical processes that cause subduction of fluid from the mixed layer into the thermocline and the outflow from the thermocline are assumed to continue exactly as before the surface warming. This simple warming (at constant salinity) decreases the density of fluid parcels in the mixed layer so that when an individual parcel is subducted, it does so along a less dense surface than it would have done in the absence of warming. This process of "pure warming subduction" was used by Church et al. (1991) in a model of the sea level rise caused by ocean thermal expansion. Here we elaborate on the justification for this physical model.

We consider a scenario of this warming and subduction process from the viewpoint of a simple fluid parcel as depicted in Fig. 1. In the cross section of Fig. 1a, an individual parcel that would normally have joined the thermocline at a density of ρ_1 is warmed (at a given salinity) and is subducted into the thermocline along the less dense horizon, ρ_2, as shown. Because this parcel is not subducted along the ρ_1 density surface, all the fluid between the two density surfaces will be displaced downward slightly in the water column. In the S–θ diagram of Fig. 1b, the warmed parcel has the properties (S_2, θ_2) and this parcel lies on the same density surface as water of the original thermocline with properties (S_3, θ_3). Now consider the average properties of fluid between the ρ_1 and ρ_2 density surfaces where on the one hand the parcel is subducted along the initial height of the ρ_1 density surface without any extra warming, and on the other hand it is warmed and subducted along the ρ_2 density surface. During the above sequence of warming and subduction, the isopycnals both below ρ_1 and above ρ_2 (see Fig. 1a) do not move. The volume-averaged salinity of the fluid, averaged over all the affected fluid, is the same in both cases, while the average potential temperature of this fluid will be different. In this way the average S–θ properties will change from (S_4, θ_4) to (S_5, θ_5) under this pure warming scenario. Parcel 6 of the original thermocline has the same density as this new fluid. It is interesting to note that the warming and subsequent subduction has caused the average fluid properties, (S_5, θ_5), to be *cooler* (and fresher) than the original thermocline fluid at the same density (S_6, θ_6). This counterintuitive result was described in Church et al. (1991).

We conclude that the surface warming at constant salinity, followed by subduction, is equivalent to

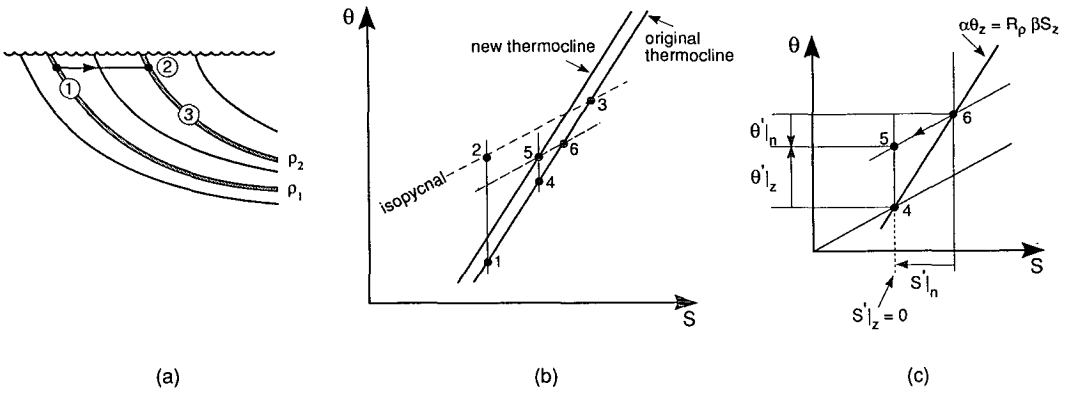

FIG. 1. The warming process. (a) Parcel 1 is warmed at constant salinity so that it attains the properties of point 2, which has the same density as parcel 3. (b) Upon subduction, parcel 2 joins the thermocline at the density of parcel 3 of the original thermocline. The average properties of all the fluid between ρ_1 and ρ_2 of (a) is at point 4 in (b) and moves to point 5 under this purely warming subduction scenario. Note that $S_5 = S_4$ and that parcel 6 of the old thermocline has the same density as the cooler and fresher parcel 5 of the new thermocline. Warming at the sea surface has caused the water mass to cool and freshen when viewed along a constant density horizon. (c) Shows an enlargement of part of (b).

warming thermocline fluid parcels at a given depth without a change in salinity. This has been found above by considering the average of fluid properties over the depth range from ρ_1 to ρ_2. Is this depth averaging an issue? We believe it is not for the following reasons. The warming of surface water due to the climate change may be up to 0.05°C/yr, and using a value of N^2 (square of the buoyancy frequency) of as little as 10^{-5} s^{-2}, the depth between the two density horizons is only 10 m. By comparison, diffusion over the course of a single year has the ability to smooth fluid properties in the vertical by ±20 m (using a vertical diffusivity of 10^{-5} m^2 s^{-1}). Also, the surface warming is expected to affect much more of the water column than just 10 m, and the pair of density surfaces shown in Fig. 1 is part of a continuous sequence of pairs occurring through the water column. Hence we are justified in considering the "warming only" subduction process to operate at a given depth or at a given density level, rather than having to consider separately the decrease of volume of the layer from which parcel 1 was extracted, the increase of volume of the layer into which parcel 2 is injected, and the increase in depth of the fluid in between.

By extending our scenario to every parcel in the water column shown in Fig. 1, each individual parcel of the thermocline is warmed at constant salinity, so that the whole S–θ relation for the thermocline is shifted vertically upward in Fig. 1b. The two essential characteristics of the "pure warming" scenario are (i) that the salinity of the water column is unchanged at a given depth and (ii) that the potential temperature increases at a given depth. These characteristics are used in section 3 to develop a signature of the warming process in terms of the observed property changes, including the fact that if the vertical gradients of potential temperature and salinity are both positive, then the potential temperature and salinity both decrease along neutral surfaces.

From the work of Walin (1982), Tziperman (1986), and Speer and Tziperman (1992) it can be shown that the subduction rate per unit horizontal area (which scales as a downward vertical velocity), averaged over the area of the ocean with mixed-layer density between ρ and $\rho + d\rho$, is given by $(-\rho/g)(B^{\text{net}}A_\rho)_\rho/A_\rho$, where A_ρ is the rate of change of the horizontal area of the ocean with respect to sea surface density, and B^{net} is the surface heat flux (less the heat flux that is lost to lateral advection in the Ekman layer). In this way our microcosm of Fig. 1 is similar to what would be produced by a delta function of warming at one sea surface density. This relation for the subduction rate shows that there would be an upwelling of water at one density and a subduction of water at a slightly lower density, similar to our process as depicted in Fig. 1.

b. *Pure freshening*

Here we consider freshening of the mixed layer, while, at the same time, the temperature of the mixed-layer fluid is unchanged. One may expect more realistically that the mixed layer fluid will be both warmed and freshened in the Southern Ocean for increasing atmospheric CO_2 since the coupled atmosphere–ocean model of Manabe et al. (1991) shows increased precipitation over evaporation south of 45°S. This freshwater flux results in freshening of the surface waters by 0.2 psu. In the same area of the model the increase in surface temperature ranges over 0° to 2°C from 65° to 45°S. Therefore, in the surface mixed layer of the Southern Ocean of their model, salinity changes account for more than half the density change caused by

their predicted temperature increase. It is therefore important to allow for the changes in the salinity field at high latitudes when interpreting hydrographic observations in terms of climate change.

The labeling of the fluid parcels in the "pure freshening" scenario of Fig. 2 follow closely those of the previous section. Suffice to say that the net observable result of the sequence of freshening and subduction is that an average fluid parcel 4 on the original thermocline is freshened at constant potential temperature to point 5 on the new thermocline S–θ curve. The figure also shows the contrast in properties, ($S_5 - S_6$, $\theta_5 - \theta_6$), along a neutral surface between the two epochs.

c. *Pure heaving*

The special cases described in the previous two subsections have assumed that the rates of subduction of fluid into and out of each pair of layers do not change. Now we allow for variations in the heights of neutral surfaces that occur in the absence of water mass change. The height variations may occur due to changes in the rate of renewal of water masses between pairs of neutral surfaces, and by changes in the patterns of wind stress. Figure 3a is a sketch of the temporal variations in the heights of neutral surfaces. While there is no signature of this process on the S–θ diagram, the process does affect observations at fixed depths. The expected sense (sign) of this process under warming is quite uncertain. Here we have considered it to be positive when the height of a neutral surface decreases with time (i.e., the surface deepens), so that the fluid at a given depth becomes less dense and hence contributes to a rise in sea level.

Our three ventilation processes seem sensible choices for interpreting data along a vertical ocean section and in this paper we use these three ventilation mechanisms as basis functions to decompose the observed temporal property changes. It should be noted however that we have not considered any dynamical constraints in our selection of these basis functions. For example, a global increase in the sea surface temperature, with no accompanying change in either sea surface salinity or wind stress, as considered by Church et al. (1991) causes a changed density field that is not in Sverdrup balance with the imposed wind stress field. As a consequence, the ocean responds with a heave motion in addition to the "pure warming." In this way, the dynamical constraints could cause a combination of our three ventilation basis functions to be observed even though the thought experiment may appear as though it would lead to only one.

3. Comparison of S and θ at constant depth and along neutral surfaces

The remarkable feature of the pure warming subduction process is that global warming causes an observed cooling (and corresponding freshening) along neutral surfaces. This was first pointed out by Church et al. (1991). The "pure freshening" process is less remarkable in that a freshening of a mixed-layer parcel leads to observed freshening (and a corresponding cooling) along neutral surfaces. These results only hold where the stability ratio, $R_\rho = \alpha\theta_z/\beta S_z$, of the water column is greater than 1. Figure 4 shows the effect of variations of R_ρ on the sign of the variations of potential temperature along a neutral surface $\theta'|_n$, for both the pure warming and pure freshening scenarios. When $R_\rho < 1$ (i.e., either a doubly stable stratification or a "diffusive" stratification) the pure warming subduction process causes an *increase* in potential temperature and salinity along neutral surfaces. The pure freshening process causes an *increase* in salinity (and in potential

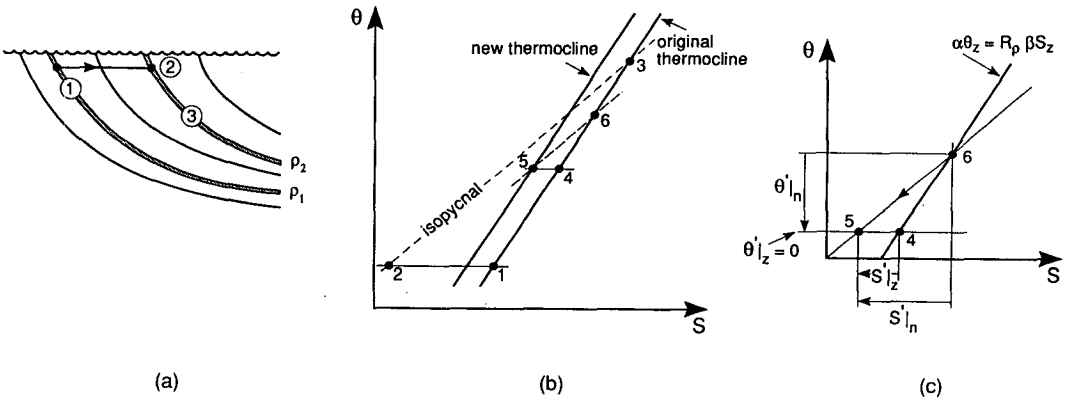

FIG. 2. The freshening process. (a) Parcel 1 is freshened at constant potential temperature so that it attains the properties of point 2, which has the same density as parcel 3. (b) Upon subduction, parcel 2 joins the thermocline at the density of parcel 3 of the original thermocline. The average properties of all the shaded fluid between ρ_1 and ρ_2 of (a) is at point 4 in (b) and moves to point 5 under this purely freshening subduction scenario. Note that $\theta_5 = \theta_4$ and that parcel 6 from the original thermocline has the same density as the cooler and fresher fluid of parcel 6 of the new thermocline. (c) Shows an enlargement of part of (b).

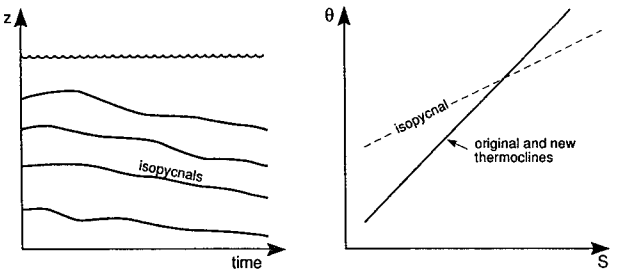

FIG. 3. Pure heaving process. These figures illustrate the third subduction process where the rates of pumping into and out of various layers change, leading to changes in the heights of neutral surfaces, but the fluid properties of water being subducted along each isopycnal are unchanged. This vertical heave of neutral surfaces can also be caused by changes in the imposed wind stress and the adjustment of the gyres via Rossby waves.

temperature) along neutral surfaces when the stability ratio is in the range $0 < R_\rho < 1$ (i.e., when the water column is stratified in the "diffusive" sense).

In addition to the signatures of the three different subduction processes on the observed change of S and θ along neutral surfaces, each process also has a signature in the changes of S and θ at constant depth. For example, in the pure warming process (Fig. 1b) neither the parcel's depth nor its salinity changes (i.e., $z_6 = z_5$ and $S_6 = S_5$) while its potential temperature increases by $\theta_5 - \theta_6$. In this section we will establish the relationships between the observed changes of S and θ, both along neutral surfaces and at constant depth, for each of the three subduction processes that we are considering.

Consider two vertical CTD casts taken at the same latitude and longitude, but separated in time (see Fig. 5). The change in a scalar quantity, ψ, at fixed depth is given by $\psi'|_z = \psi_c - \psi_a$, while the change along the neutral surface is given by $\psi'|_n = \psi_b - \psi_a$. The difference between $\psi'|_z$ and $\psi'|_n$ is equal to $-(\psi_b - \psi_c)$ and can also be expressed in terms of the change in height of the neutral surface, $\mathcal{N}'$, times the vertical gradient of ψ, ψ_z (assuming that the vertical motions are small enough so that $\psi_b - \psi_c$ can be approximated by the first term in a vertical Taylor expansion of ψ, $\mathcal{N}'\psi_z$). Writing this result for potential temperature and salinity, we have

$$\theta'|_z = \theta'|_n - \mathcal{N}'\theta_z \quad \text{and} \quad S'|_z = S'|_n - \mathcal{N}'S_z. \quad (1)$$

It is more useful to express these equations in density units by multiplying them by the thermal expansion and haline contraction coefficients, α and β, respectively, where

$$\alpha \equiv -\frac{1}{\rho}\frac{\partial \rho}{\partial \theta}\bigg|_{S,p} \quad \text{and} \quad \beta \equiv \frac{1}{\rho}\frac{\partial \rho}{\partial S}\bigg|_{\theta,p}, \quad (2)$$

giving

$$\alpha\theta'|_z = \alpha\theta'|_n - \mathcal{N}'\alpha\theta_z \quad \text{and}$$

$$\beta S'|_z = \beta S'|_n - \mathcal{N}'\beta S_z. \quad (3)$$

Along a neutral surface we know, by definition, that (McDougall 1987)

$$\alpha\theta'|_n = \beta S'|_n, \quad (4)$$

while at any height the vertical gradients, θ_z and S_z, are known, so that $\alpha\theta_z$ and βS_z are related through the stability ratio, R_ρ, defined by

$$\alpha\theta_z = R_\rho \beta S_z. \quad (5)$$

To deduce the relationships between the observed variables $S'|_z$, $\theta'|_z$, $S'|_n$, $\theta'|_n$, and $\mathcal{N}'$ for each of the three subduction processes, we examine the geometry of Figs. 1c and 2c. For the pure warming process, where $S'|_z = 0$ (or $S_5 - S_4 = 0$ in Fig. 1c), the change in potential temperature from point 4 to point 5 occurs at fixed depth, so that $\theta'|_z = \theta_5 - \theta_4$. It can be seen from the geometry of Fig. 1c [or equivalently from Eqs. (3) and (5)] that

$$(\alpha\theta'|_z - \alpha\theta'|_n) = \alpha(\theta_6 - \theta_4) = R_\rho\beta(S_6 - S_4)$$
$$= R_\rho\beta(S_6 - S_5) = -R_\rho\beta S'|_n. \quad (6)$$

Hence we have, using Eqs. (3) and (6),

$$\alpha\theta'|_z > 0, \quad \beta S'|_z = 0, \quad \beta S'|_n = \mathcal{N}'\beta S_z = \alpha\theta'|_n$$
$$= -\alpha\theta'|_z(R_\rho - 1)^{-1} \quad \text{for pure warming.} \quad (7)$$

Thus, positive pure warming in the main thermocline (where $R_\rho > 1$) requires that the freshening on neutral surfaces be balanced by the downward movement of neutral surfaces and that the cooling on neutral surfaces is proportional to the observed warming on pressure surfaces. The constant of proportionality varies with depth depending on R_ρ.

Similarly, for pure freshening, where $\alpha\theta'|_z = 0$ (or $\theta_5 - \theta_4 = 0$), from the geometry of Fig. 2c we find that $-\alpha\theta'|_n = -R_\rho\beta(S'|_n - S'|_z)$, so that

$$\alpha\theta'|_z = 0, \quad \beta S'|_z < 0, \quad \alpha\theta'|_n = \mathcal{N}'\alpha\theta_z = \beta S'|_n$$
$$= \beta S'|_z(1 - R_\rho^{-1})^{-1} \quad \text{for pure freshening.} \quad (8)$$

The vertical heaving of the water column involves no changes of S or θ along neutral surfaces, so that

$$\alpha\theta'|_n = \beta S'|_n = 0, \quad \beta S'|_z = -\mathcal{N}'\beta S_z,$$
$$\alpha\theta'|_z = -\mathcal{N}'\alpha\theta_z \quad \text{for pure heaving.} \quad (9)$$

The most important aspect of (7)–(9) is that they provide a model for quantitatively examining the relationship between changes in S–θ correlations and changes of temperature and salinity on pressure surfaces.

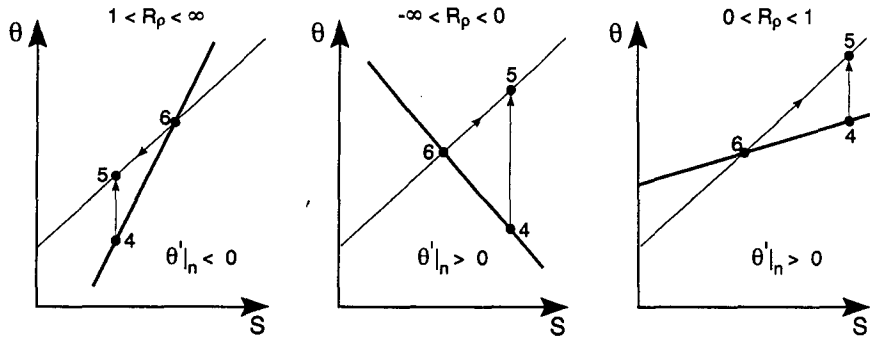

(a) Pure Warming

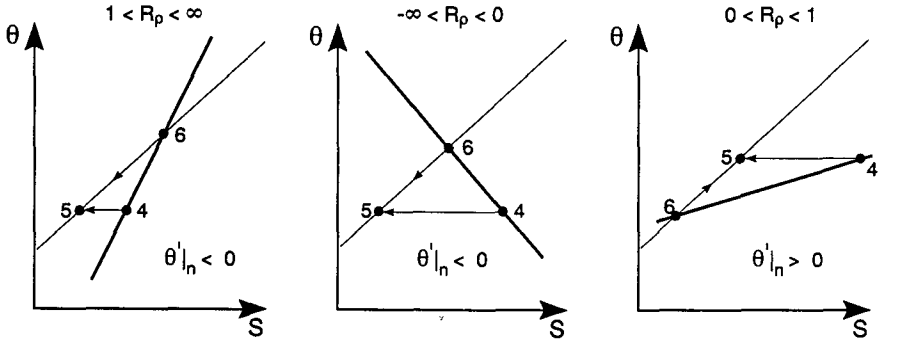

(b) Pure Freshening

FIG. 4. Sketches of the changes of properties at constant depth, $(S_5 - S_4, \theta_5 - \theta_4)$, and at constant "density" $(S_5 - S_6, \theta_5 - \theta_6)$, for various values of the stability ratio, $R_\rho \equiv \alpha\theta_z/\beta S_z$. (a) Shows three different ranges of R_ρ for the "pure warming" subduction scenario, while (b) is for "pure freshening." The faint line in each panel is an isopycnal (or neutral-density surface) and the bold line is the vertical S–θ curve. In the R_ρ range $1 < R_\rho < \infty$ the water column is susceptible to the salt fingering type of double-diffusive convection, for $-\infty < R_\rho < 0$ the water column is stably stratified in both heat and salt, while for $0 < R_\rho < 1$ the "diffusive" type of double-diffusion is possible.

These three relationships, (7)–(9), can be used to draw vectors of each subduction process on diagrams whose axes are chosen from among the observed variables $S'|_z$, $\theta'|_z$, $S'|_n$, $\theta'|_n$, and $\mathcal{N}'$. However, it is more convenient to deal in the six dimensionless variables that appear in (3), namely, $\alpha\theta'|_z$, $\alpha\theta'|_n$, $\mathcal{N}'\alpha\theta_z$, $\beta S'|_z$, $\beta S'|_n$, and $\mathcal{N}'\beta S_z$. That the two equations in (3) are satisfied reduces the number of independent variables from six to four, and the definitions (4) and (5) of the neutral surface and of the stability ratio further reduces the number of independent variables to two. This means that while there are many pairs of parameters to choose as the axes for a plot, any pair should contain the same information (except for the two degenerate pairs [from (4) and (5)], $\alpha\theta'|_n$ and $\beta S'|_n$, $\mathcal{N}'\alpha\theta_z$ and $\mathcal{N}'\beta S_z$, where all the data lie on a line (for a constant R_ρ).

It is convenient now to use Eqs. (3)–(5) to obtain several expressions for the change of in situ density at constant z (or at constant pressure); namely,

$$\begin{aligned}\rho^{-1}\rho'|_z &\equiv \beta S'|_z - \alpha\theta'|_z \\ &= -(R_\rho - 1)(\beta S'|_z - \beta S'|_n) \\ &= -(1 - R_\rho^{-1})(\alpha\theta'|_z - \alpha\theta'|_n) \\ &= (R_\rho - 1)\mathcal{N}'\beta S_z \\ &= (1 - R_\rho^{-1})\mathcal{N}'\alpha\theta_z. \end{aligned} \tag{10}$$

4. Decadal and seasonal changes in the hydrography from the Tasman Sea

In this paper, we examine the differences of potential temperature and salinity on neutral surfaces and on

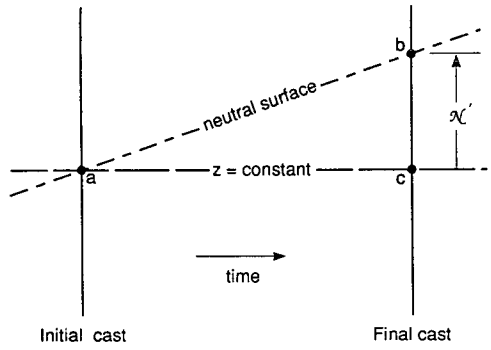

FIG. 5. A sketch showing two casts from the same latitude and longitude, but separated in time. Points a and c are at the same depth on both casts, and points a and b lie on the same neutral surface; that is, loosely speaking, they have the same "density." Here $\mathcal{N}'$ is the change in the height of the neutral surface over this time interval. The change of a scalar quantity, ψ, along the neutral surface is related to the change at constant depth by $\psi'|_z = \psi'|_n - \mathcal{N}'\psi_z$.

isobars from data that are separated in time by 6 months and 23 years. The main aim here is to determine whether the reported climate change (Bindoff and Church 1992) can be characterized in terms of the three processes described in sections 2 and 3. Inverse methods are applied to objectively find the proportion of each process that is present.

a. Treatment of data

Hydrographic data from the SCORPIO sections in the Tasman Sea at 43°S (obtained in March 1967) (Stommel et al. 1973; Warren 1973) are used with repeat sections taken in September 1989 and March 1990 by the RV *Franklin*. These three realizations are probably the best quality repeat sections available in the Southern Hemisphere.

Because the casts in these repeat sections do not coincide in space, they have been objectively mapped onto the exact locations of the SCORPIO casts (Fig. 6). The objective mapping techniques reduce the effects of (i) aliasing of eddy noise into the long wavelength signal, and (ii) biases in the hydrographic properties due to sampling differences between the two sections. The data from both of the Franklin and the SCORPIO cruises were interpolated onto a regular set of standard depths consistent with the spacing of the SCORPIO bottle data. In this case, a two-step procedure has been used to obtain the objectively mapped field similar to that used by Roemmich (1983). In the first step a Gaussian covariance function is used with large horizontal and vertical scales to find a realistic estimate of the large-scale mean field. In the second step, using the same covariance function, the horizontal and vertical scales are reduced to 300 km and 3 standard depths, respectively, so that fine-scale features such as eddies are resolved, albeit with smaller amplitude.

The relations obtained in section 3 for pure warming, pure freshening, and pure heave are local relations valid at a point in space. However, to increase statistical reliability of the interpretation it is necessary to average over a number of casts. Equations (3) (for θ' and S') both involve the thermal expansion and salinity contraction coefficients α and β, both of which are functions of θ, S, and pressure p. The nonlinear dependence of these coefficients on the in situ fields means that averaging of the terms in the equations must be carefully done so that the averaged casts still lie on the same neutral surface defined by Eq. (4).

The hydrographic data from each cruise were labeled with "neutral density," γ^n, using an algorithm developed by Jackett and McDougall. A surface of constant γ^n has the neutral property [defined by Eq. (4)] that fluid parcels can be exchanged over a small distance along the surface without experiencing a resulting buoyancy force. At the end of this labeling step, each "bottle" on each cast had a salinity, a potential temperature, a pressure, and a neutral density, γ^n. Here $\mathcal{N}'$ is the difference in height between the same surface at two time instants, where positive values correspond to upward movements of the surface. In this analysis averages have been calculated along neutral surfaces in the following way to preserve the neutral surface definition (in time and space) between the average of the casts at 43°S and for each realization (that is, 1967, 1989, and 1990). Averaging the terms in Eq. (3) (in this discussion we concentrate on the potential temperature field) gives

$$\langle \alpha\theta'|_z \rangle = \langle \alpha\theta'|_n \rangle - \langle \mathcal{N}'\alpha\theta_z \rangle, \qquad (11)$$

where the $\langle\ \rangle$ operator denotes an average along a neutral surface across the Tasman Sea. The first term on the right-hand side of (11) is evaluated by

$$\langle \alpha\theta'|_n \rangle = \langle \alpha(\theta_m, S_m, p_m)[\theta^f|_n - \theta^i|_n] \rangle, \qquad (12)$$

where $p_m = \frac{1}{2}[p^f|_n + p^i|_n]$, $\theta_m = \frac{1}{2}[\theta^f|_n + \theta^i|_n]$, and $S_m = \frac{1}{2}[S^f|_n + S^i|_n]$ are the average pressure, potential temperature, and salinity of the same neutral surface at the initial (i) and final (f) times at a given horizontal location. The use of the average in time of potential temperature, salinity, and pressure is consistent with the numerical methods used to obtain neutral surfaces (see McDougall and You 1990). The term on the left-hand side of (11) is evaluated as

$$\langle \alpha\theta'|_z \rangle = \langle \alpha(\theta_m, S_m, p_m)[\theta^f(p_m) - \theta^i(p_m)] \rangle, \qquad (13)$$

while the third term is evaluated as

$$\langle \mathcal{N}'\alpha\theta_z \rangle = \frac{1}{2}\langle \mathcal{N}'\alpha(\theta_m, S_m, p_m)[\theta^f_z(p_m) + \theta^i_z(p_m)] \rangle, \qquad (14)$$

where θ_z on the left-hand side is the average vertical gradient of the potential temperature field linearly interpolated to the time average depth p_m. In addition

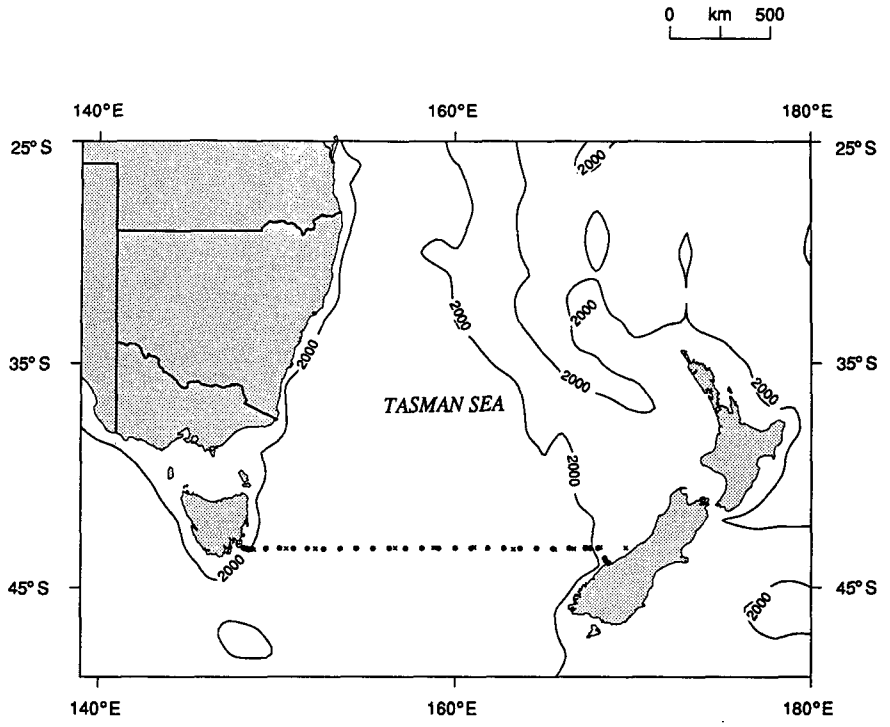

FIG. 6. The locations of the SCORPIO data (shown by the crosses) and the Franklin data (shown by the dots) used in this analysis at 43°S.

to these three terms, the models of warming and freshening depend on the stability ratio, R_ρ. For our purposes, the appropriate way to form the stability ratio for a complete ocean section is

$$R_\rho = \frac{\langle \mathcal{N}' \alpha\theta_z \rangle}{\langle \mathcal{N}' \beta S_z \rangle} = \frac{\langle \alpha\theta'|_z \rangle - \langle \alpha\theta'|_n \rangle}{\langle \beta S'|_z \rangle - \langle \beta S'|_n \rangle}. \quad (15)$$

In addition to calculating the sectional average terms $\alpha\theta'|_z$, $\alpha\theta'|_n$, $\mathcal{N}'\alpha\theta_z$, $\beta S'|_z$, $\beta S'|_n$, and $\mathcal{N}'\beta S_z$ (the angle brackets are henceforth dropped), estimates of the random noise for each of these terms was also determined. The rms estimates of the noise allow confidence intervals to be calculated for the sectional average terms shown in Fig. 7. The rms noise in each of the six terms is estimated directly from the two mapped repeat sections at 43°S obtained in September 1989 and March 1990 using the relation

$$\sigma^2_{\text{a priori}} = \frac{1}{2n} \sum_{i=1}^{n} (d_i^f - d_i^i)^2, \quad (16)$$

where the term $d_i^f - d_i^i$ is the difference field on the same neutral surface and geographic location separated by six months, and n is the number of differences on each neutral surface. This procedure for estimating the noise is much simpler than formally propagating the errors in the temperature and salinity fields obtained from the objectively mapped data on the SCORPIO grid. The 90% confidence interval of the mean differences on neutral surfaces (Fig. 7) follows standard methods (e.g., Bendat and Piersol 1986), and takes into account the degrees of freedom and the error in forming the difference fields. Effectively there was approximately one degree of freedom per eddy diameter across the section.

The difference fields in the upper water column (γ^n = 26.6 to 27.6 kg m^{-3}) are coherent across the whole Tasman Sea, consistent with the observations of Bindoff and Church (1992). For space reasons, only the potential temperature differences ($\alpha\theta'|_n$) across the Tasman Sea on neutral surfaces is shown in Fig. 8. The largest decrease in $\alpha\theta'|_n$ occurs in the western side of the Tasman Sea, decreasing to the east. The other fields with significant differences at the 90% level, shown in Fig. 7, also have similar basinwide patterns.

The average difference along the 43°S section between the RV *Franklin* 1990 and SCORPIO data (each observed in the same season) show highly significant differences in both the potential temperature and salinity fields on neutral and isobaric surfaces (Figs. 7a and 7b). The difference terms $\alpha\theta'|_z$ and $\alpha\theta'|_n$ are equivalent to the results presented in Figs. 2a and 3a of Bindoff and Church (1992). The changes in temperature and salinity can be approximately scaled from Fig. 7 using $\alpha \sim 2 \times 10^{-4}$ and $\beta \sim 0.75 \times 10^{-3}$. The changes in temperature and salinity on neutral surface 26.8 are quite large, 0.6°C and 0.15 psu.

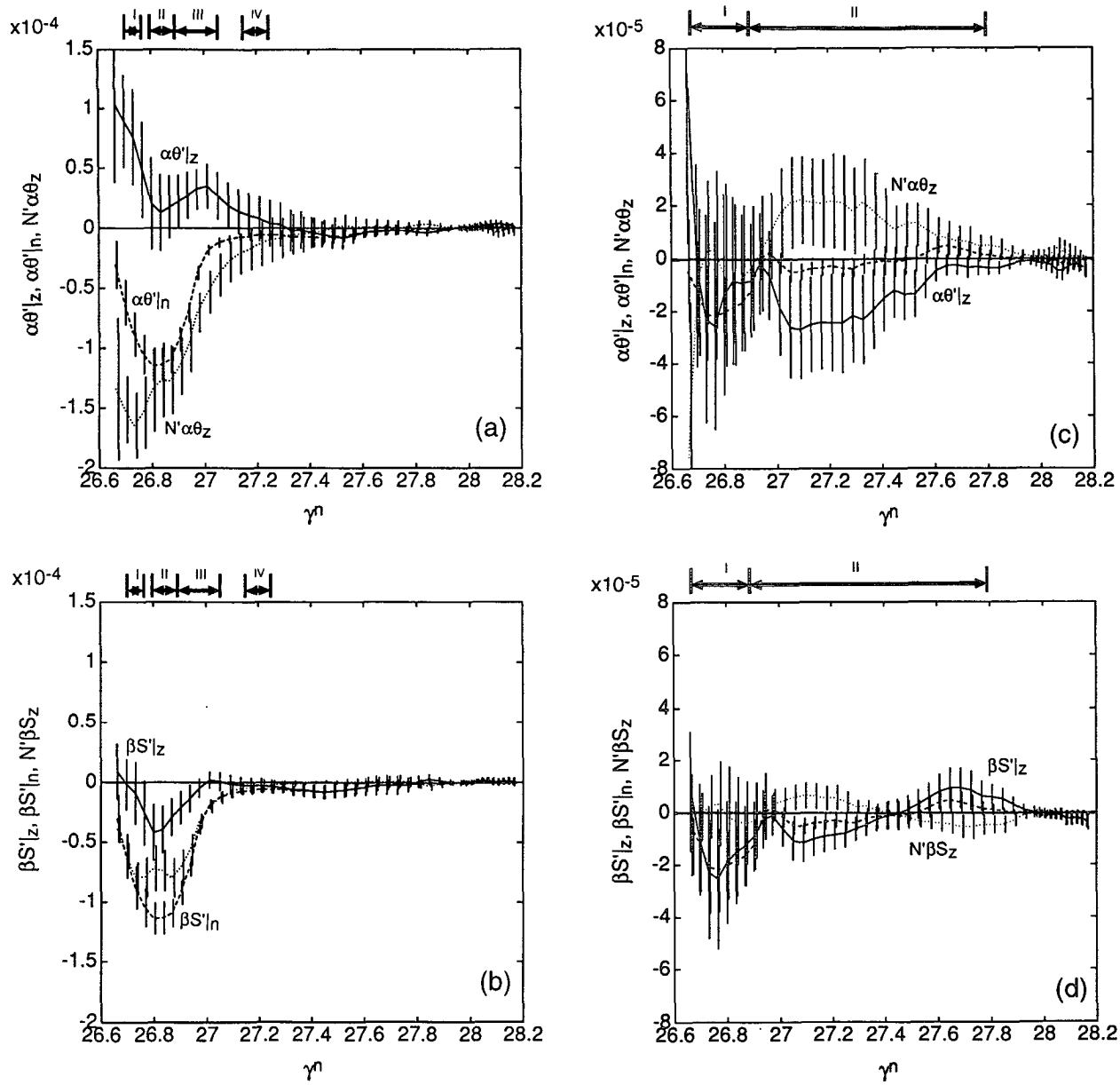

FIG. 7. Graphs of $\alpha\theta'|_z$, $\alpha\theta'|_n$, $\mathcal{N}'\alpha\theta_z$, $\beta S'|_z$, $\beta S'|_n$, and $\mathcal{N}'\beta S_z$ as a function of neutral density. (a) and (b) Differences between *Franklin* 1990 and SCORPIO data. (c) and (d) Differences between summer 1990 and winter 1989 *Franklin* data. The continuous, dashed, and dotted lines correspond in (a) and (c) to $\alpha\theta'|_z$, $\alpha\theta'|_n$, $\mathcal{N}'\alpha\theta_z$, and in (b) and (d) to $\beta S'|_z$, $\beta S'|_n$, and $\mathcal{N}'\beta S_z$. The error bars are 90% confidence intervals on each of the mean difference fields. Note the different scales for (a), (b) and (c), (d).

In the density range $\gamma^n = 26.6$ to 27.2 the sectional differences show warming on isobaric surfaces (i.e., positive changes), cooling of potential temperature on neutral surfaces (i.e., negative changes), and small changes in salinity on isobars, suggestive of pure warming. On density surfaces $\gamma^n = 27.2$ to 27.6, the 23-year differences are suggestive of the freshening scenario with small changes in potential temperature and significant freshening on both neutral and isobaric surfaces.

The confidence intervals are of interest in their own right. They characterize the noise level primarily due to eddies in the data separated by six months. In the upper thermocline, properties on neutral surfaces have smaller confidence intervals by a factor of 2 compared to the terms observed on isobars or the terms that depend on the movement of density surfaces. These smaller confidence intervals in the thermocline result from the way eddies perturb isotherms and density surfaces. In the upper thermocline, mesoscale eddies

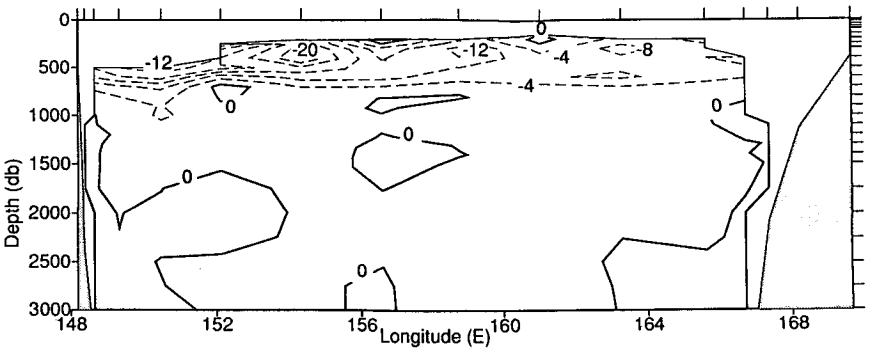

FIG. 8. The difference field of $\alpha\theta'|_n$ between *Franklin* 1990 and SCORPIO data as a function of depth for the 43°S section in the Tasman Sea. The contour interval is 4×10^{-5}. The largest contour of -20×10^{-5} corresponds to a change in potential temperature on neutral surfaces, $\theta'|_n$, of approximately −1.15°C.

cause large vertical movements of isotherms, while density surfaces tend to follow isotherms (and isohalines). As a result, the variation of potential temperature on isobars is large compared with its variation on density surfaces. Thus, as suggested by Bindoff and Church (1992), the use of density surfaces in the thermocline increases the sensitivity of the observations for diagnosing climate change by reducing the noise associated with eddies. However, below the salinity minimum the noise is more equally distributed between each of the six variables and, in this case, properties on neutral surfaces have no statistical advantage over isobaric surfaces.

b. *Hodographs of warming, freshening, and heaving*

The simplest method for diagnosing the relationship between each of the observed variables $\alpha\theta'|_z$, $\alpha\theta'|_n$, $\mathcal{N}'\alpha\theta_z$, $\beta S'|_z$, $\beta S'|_n$, and $\mathcal{N}'\beta S_z$ and each of the three processes is by the use of hodographs where one variable is plotted against another. Figure 9 shows such hodographs for the 23 year and 6 month differences from the Franklin and SCORPIO data for two pairs of variables. Each data point on these hodographs (the continuous lines with points labeled $a, b, \ldots, t$) is from a different neutral surface, and can be viewed as a linear combination of the three processes. These processes are represented by vectors (of unknown length but with a well-defined slope) from the origin to points along the straight or curved lines labeled Warming, Freshening, and Heave. For graphs between the variables $\beta S'|_n$ and $\mathcal{N}'\beta S_z$ (Figs. 9a and 9c), pure warming vectors fall along the line labeled "Warming" with a slope of 45° (see Fig. 8). Pure heave has no change of salinity on neutral surfaces and thus vectors representing this process lie along the horizontal axis (labeled Heave). Pure freshening has a slope of R_ρ on these graphs, and each point on the pure freshening line (the curved dashed line labeled $a, b, \ldots, t$) represents a vector drawn from the origin to the labeled point. The faint dashed vector is an example of such a vector drawn from the origin to the neutral surface b. Because of the variation of R_ρ with each successive surface, the pure freshening vector has a more complex pattern than the other two processes. The length of the vectors for each of these processes is arbitrary. Figures 9b and 9d are similarly drawn but using $\alpha\theta'|_z$ and $\alpha\theta'|_n$ as the hodograph axes. Now the pure warming vector has a slope of $-(R_\rho - 1)^{-1}$, whereas pure freshening and heave are represented by orthogonal lines along vertical and horizontal axes, respectively. Note that on both Figs. 9a and 9b, points a and k are consistent with pure warming alone with no need to invoke freshening or heave.

For the upper 1000 db of the 43°S section θ_z, S_z and $(R_\rho - 1)$ are all positive, and the direction of the vectors represented by the labeled lines are for positive changes of pure warming, pure freshening, and pure downward heave.

In this section we choose to interpret the hodographs in terms of the dominant process. In other words, an observation that lies in the direction of one of the three pure processes is regarded as dominating. For example, on Fig. 9b the line from the origin to the points labeled "a" and "b" is almost parallel to the corresponding "pure warming" vectors (also labeled "a" and "b"). The changes of $\alpha\theta'|_n$ and $\alpha\theta'|_z$ on these surfaces are characterized by pure warming. This "simplicity" criterion is quite different from that used in the inverse problem of minimizing the norm of the proportion of each process, described in the next section.

1) THE DIFFERENCES OVER 23 YEARS

Using the simplicity criterion, the hodographs of the difference between the *Franklin* and SCORPIO data (Figs. 9a and 9b) can be interpreted deterministically and the issues of the accuracy and resolution of each process is left to the next section. In moving down the water column, we have chosen to discuss the changes

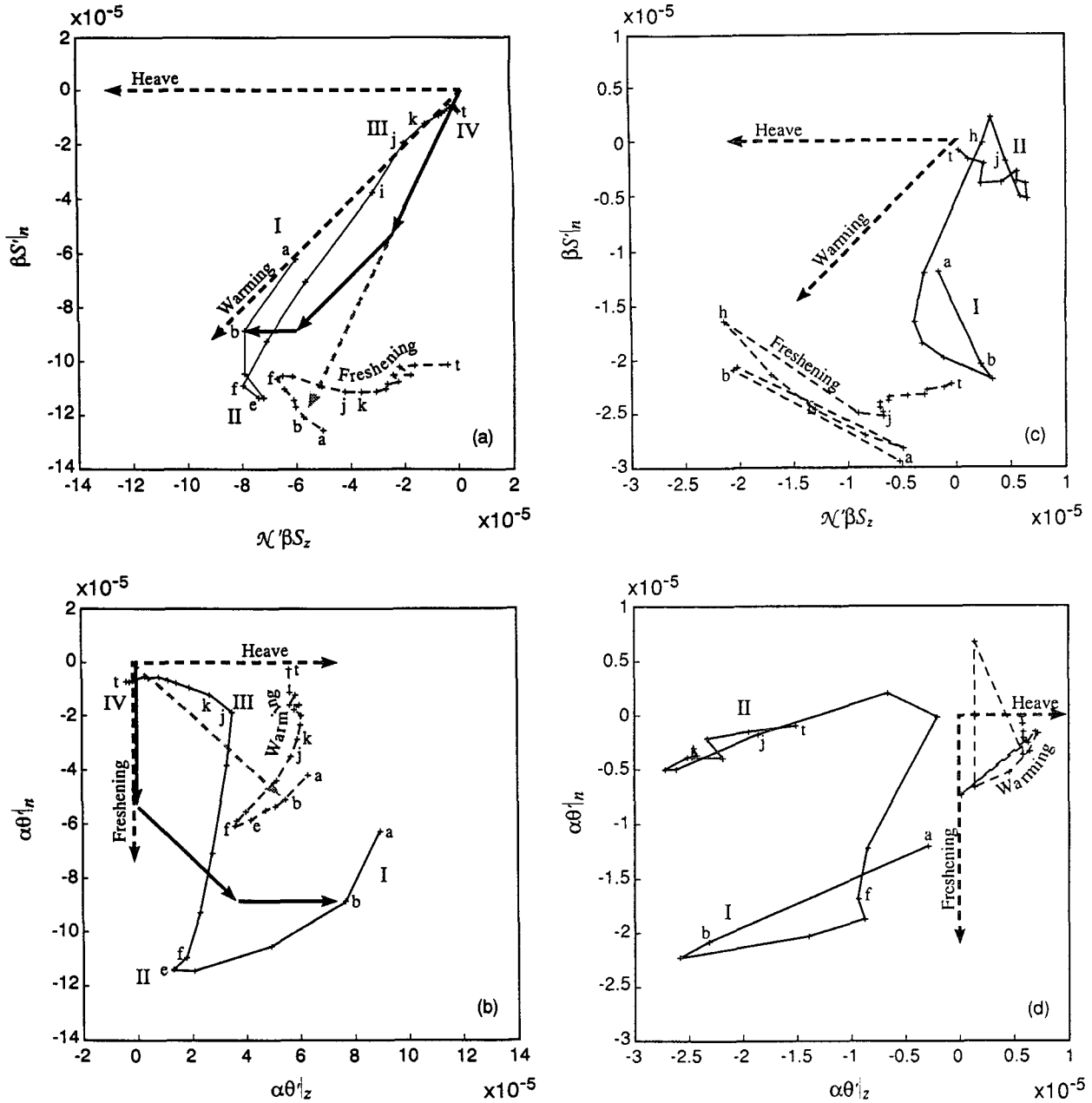

FIG. 9. Hodographs of the labeled variables for successive neutral surfaces. The continuous line (labeled with $a, b, \ldots, t$) is the observation for each surface down to the salinity minimum (approximately 1000 db). Points on the straight or curved dashed lines labeled Warming, Freshening, and Heave represent vectors drawn from the origin along which positive changes of pure warming, pure freshening, and pure downward heave lie, respectively. (a) and (b) Average differences between the *Franklin* 1990 and SCORPIO data. (c) and (d) Average differences between summer 1990 and winter 1989 *Franklin* cruises. The labels I, II, III, and IV identify the distinct regions where a single process dominates (Table 1). The three bold vectors in (a) and (b) are the contribution of pure freshening, pure warming, and pure heave from the solution of Eq. (17) with two eigenvalues. The sum of these three vectors is the observation on neutral surface b. The vector for pure freshening in (a) and (c) does not have a fixed angle on these diagrams but depends on R_ρ. Similarly, in (b) and (d), the vector for pure warming has a slope that depends on R_ρ.

in terms of four regimes, labeled I to IV (Table 1). In the first regime, the hodograph lies parallel to the pure warming axis; that is, $\mathcal{N}'\beta S_z$ is approximately equal to $\beta S'|_n$ on these neutral surfaces [see (7)]. The second regime is dominated by freshening in the upper part of the thermocline. Here the downward movement of the neutral surfaces, $R_\rho \mathcal{N}'\beta S_z$, is balanced by freshening $\beta S'|_n$ [see (8) and (5)]. Below this freshening

TABLE 1. The regimes, defined by neutral density, surface label (a–z), and depth, where a single or a pair of processes dominate the decadal and seasonal difference fields. The first part of the table is for the difference between *Franklin* 1990 and SCORPIO data, while the second part is for the difference between summer 1990 and winter 1989 *Franklin* data. The column in this table headed "Approximate ρ_θ" contains the approximate values of potential density (referred to the sea surface) that correspond to the neutral densities.

Regime	γ^n (kg m^{-3})	Approximate ρ_θ	Surfaces	Depth (db)	Process
		Decadal differences			
I	26.69–26.76	26.64–26.70	a–c	190–245	Warming
II	26.79–26.90	26.73–26.82	d–g	280–430	Freshening
III	26.90–27.20	26.82–27.08	g–o	430–840	Warming
IV	27.30–27.40	27.17–27.25	q–t	930–1060	Freshening
		Seasonal differences			
I	26.66–26.95	26.62–26.87	a–h	180–500	Freshening/Heave
II	26.95–27.80	26.87–27.59	h–z	500–1660	Heave

regime, warming dominates because point j on the continuous curve (i.e., the data) is parallel to the warming vector, rather than the freshening or heave vectors. Below this there is freshening again just above the salinity minimum. Below the fourth regime there is the suggestion of heave where $\alpha\theta'|_z$ is much larger than $\alpha\theta'|_n$.

The sea level change contribution for each of the four regimes can also be inferred from Fig. 9 and all of the changes in each regime make $\rho^{-1}\rho'|_z$ negative. This can be seen using (10) and that $R_\rho - 1$ is positive above the salinity minimum [so that $(R_\rho - 1)\mathcal{N}'\beta S_z < 0$].

2) THE DIFFERENCE BETWEEN SUCCESSIVE SEASONS

The hodographs of seasonal variation, between the *Franklin* 1990 and 1989 repeat cruises show a distinctly different character from the 23-year differences (Figs. 9c and 9d compared with Figs. 9a and 9b), reflecting the different processes that operate on decadal and seasonal time scales. In absolute terms the seasonal changes are much smaller (by a factor of ~5) than the 23-year changes on the shallow neutral surfaces. Two distinct regimes can be identified in the hodographs for the near surface and main thermocline waters (Table 1). The hodographs are summer minus winter differences and should have the same sense as warming. But, in both regime I and II the data show cooling ($\alpha\theta'|_z < 0$) on this time scale (Fig. 9d).

The hodographs of the data for the first depth regime are not parallel to any one single process (unlike the 23-year differences) but require a linear combination of at least two of the processes. It is significant that in this depth regime the sea level rise term, $(R_\rho - 1)\mathcal{N}'\beta S_z$, is small compared with the changes in water mass properties, $\alpha\theta'|_n = \beta S'|_n$. It would appear likely, from Fig. 9d, that increased freshening (increased precipitation) and negative heave can account for the observed differences. In contrast to regime I, the second depth regime has cooling on isobars not accompanied by changes in neutral surface temperature (i.e., $|\theta'|_z| \gg |\theta'|_n|$), which clearly implicates the heave process (see Fig. 9d). This is a pleasing result, since it would be surprising if changes of θ and S on neutral surfaces could change significantly at these depths in just six months.

5. Evaluation of the three subduction mechanisms using an inverse approach

The three ventilation models, as expressed by (7), (8), and (9) give linear relations between the six "observable" quantities $\alpha\theta'|_z$, $\alpha\theta'|_n$, $\mathcal{N}'\alpha\theta_z$, $\beta S'|_z$, $\beta S'|_n$, and $\mathcal{N}'\beta S_z$. Each of these six quantities is due to a linear combination of the three subduction mechanisms, and these relationships can be written in matrix form $\mathbf{MA} = \mathbf{d}$, or more fully as

$$\frac{\rho^{-1}\rho'|_z}{(R_\rho - 1)} \begin{bmatrix} -(R_\rho - 1) & 0 & -R_\rho \\ 1 & R_\rho & 0 \\ R_\rho & R_\rho & R_\rho \\ 0 & (R_\rho - 1) & -1 \\ 1 & R_\rho & 0 \\ 1 & 1 & 1 \end{bmatrix} \times \begin{bmatrix} A^w \\ A^f \\ A^h \end{bmatrix} = \begin{bmatrix} \alpha\theta'|_z \\ \alpha\theta'|_n \\ \mathcal{N}'\alpha\theta_z \\ \beta S'|_z \\ \beta S'|_n \\ \mathcal{N}'\beta S_z \end{bmatrix}, \quad (17)$$

where the three columns represent the effects of the pure warming, pure freshening, and pure heave processes, respectively, on the six observable quantities, and A^w, A^f, and A^h are the proportions of each process. For simplicity, the averaging operators have been omitted. In this system the weighting for each process is such that equal values of A^w, A^f, and A^h give equal contribution to sea level rise, $\rho^{-1}\rho'|_z$. This choice is

based on the premise that we have no a priori knowledge of the relative strength of the three processes.

a. *Underdetermined solution*

Although there are more equations than unknowns, this linear system is rank deficient and is formally underdetermined. The rank deficiency can be easily seen by inspecting rows for linear dependence. The main advantage of combining the temperature and salinity into a single combined system is not to increase the rank, but rather to examine all six observables simultaneously in terms of the three processes. This linear system was solved on each neutral surface using singular value decomposition (SVD) (e.g., Menke 1984) with two eigenvalues retained (the maximum allowed). In this analysis the matrix in Eq. (17) is ill-conditioned on some neutral surfaces. In obtaining the solution, each column of Eq. (17) was weighted by its norm as described by Wunsch et al. (1983) in order to improve the condition number. On surfaces where the matrix equation is well posed the column weighting has no effect on the 2 eigenvalue solution.

For the 23-year differences obtained from the inversion of (17) for rank 2 (Fig. 10a), the size of each process can be directly contrasted with that inferred from Figs. 9a and 9c. Model solutions for rank 2 were also found for the differences between the *Franklin* 1989 and SCORPIO data and the results for each process were similar to the superimposition of the results for the 23-year and 6-month differences described here. In contrast to section 4, linear combinations of processes dominate rather than a single process. Between neutral density surface 26.69 and 26.93 (regimes I and II) the model gives a linear combination of warming and freshening: both of these processes are significant at the 90% level. The approximate values of potential density that correspond to these values of neutral density are given in Table 1. For these two regimes the role of heave is less important. Below, in regime III, both pure warming and heave are stronger than pure freshening, and in regime IV pure freshening is the largest process. Thus, the minimum-norm solution emphasizes the collinear nature of the processes and the relative freedom in choosing the contribution of each process to explain the observations. As an example, the vector sum of the three processes at 217 db ($\gamma^n = 26.73$) are superimposed on the 23-year difference hodographs (Figs. 9a and 9b). Although the proportion of each mode is such as to minimize the length of the model norm, it occurs at the expense of the simplicity of the interpretation in terms of a single process.

Although it is not possible to interpret these results in terms of a single process, the general results remain. For example, the solution to the underdetermined problem shows that throughout the water column the density anomaly $\rho^{-1}\rho'|_z$ has decreased and each density level contributes to a rise in sea level over the past 23 years. Also, the solution of the SVD for each of the three subduction mechanisms has the correct sign for global warming, that is, the values in Fig. 10a are all negative above the $\gamma^n = 27.4$ surface. By contrast, the underdetermined inversion for the seasonal differences

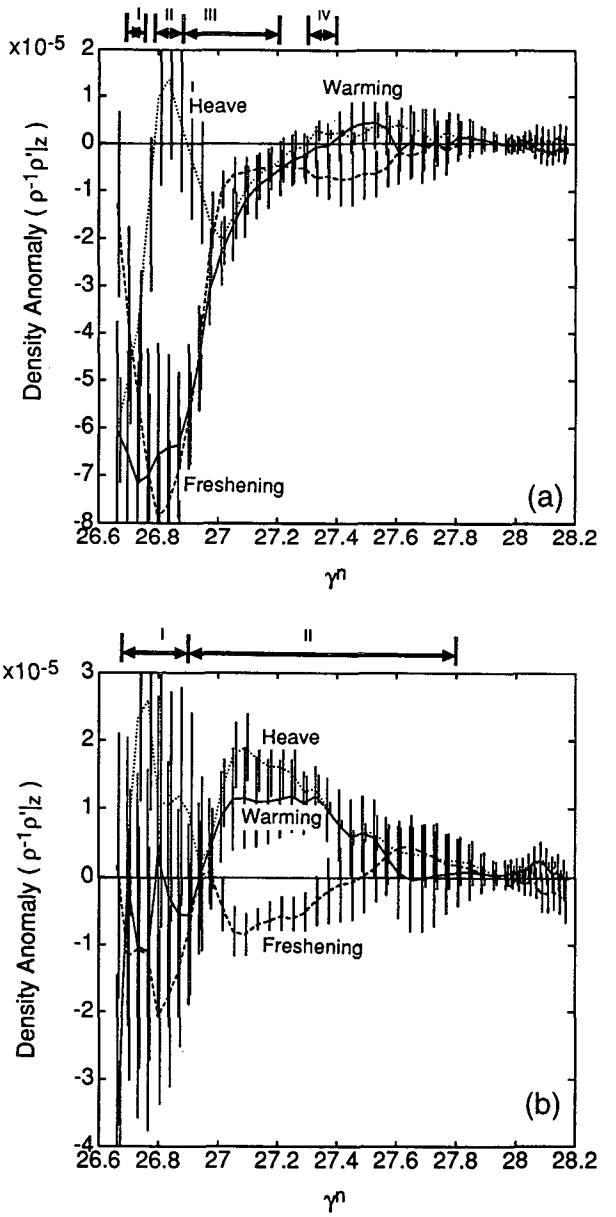

FIG. 10. The density anomaly, $\rho^{-1}\rho'|_z$, contributed by each process for the rank 2 system of the SVD solution to (17), (i.e., $A^w\rho^{-1}\rho'|_z$, $A^f\rho^{-1}\rho'|_z$, $A^h\rho^{-1}\rho'|_z$), as a function of neutral density, γ^n: (a) differences between *Franklin* 1990 and SCORPIO data, (b) differences between 1990 and 1989 *Franklin* data. The continuous, dashed, and dotted lines are the strengths of warming, freshening, and heave, respectively. The vertical bars are the 90% confidence intervals for each process.

(*Franklin* 1990 minus *Franklin* 1989) at rank 2 are often inconsistent with the sense of warming, since the warming and heave processes are positive over much of the water column in Fig. 10b. In this seasonal difference solution the waters in regime I (γ^n from 26.66 to 26.95) have freshening balancing the *upward* heave of the neutral surfaces, creating only a small change in density. In regime II (γ^n from 26.95 to 27.6) *upward* heave and cooling on isobars dominate the changes in density anomaly.

b. *Single-process solutions*

The minimization of the model norm ($\mathbf{A}^T\mathbf{A}$) in (17) has the effect of distributing the variance between each process needed to explain the data (Fig. 7). This contrasts with section 4 where the interpretation was based on the simplicity argument of using the minimum number of processes that seemed to be required by the data. In this section we extend the "simplicity" approach used in section 4 to the inverse approach. By making the additional assumption that only a single process is present (i.e., setting two of A^w, A^J, or A^h to zero), an overdetermined solution can be obtained to (17). In this case the residual between the estimated field and the observations is nonzero; and the proportion of variance, R^2, explained by a single process is defined as

$$R^2 = \frac{\mathbf{d}_{\text{est}}^T \mathbf{d}_{\text{est}}}{\mathbf{d}^T \mathbf{d}}, \tag{18}$$

where $\mathbf{d}$ is the column vector of six observables on each neutral surface and $\mathbf{d}_{\text{est}}$ is the estimated field from the overdetermined solution of (17) with only a single process.

1) THE 23-YEAR DIFFERENCES

For the 23-year differences, the R^2 value for each process defines four depth regimes where more than 95% of the variance of the data is explained by a single process (Fig. 11a). These four regimes are the same as those defined in section 4 (see Table 1) and define a sequence of pure warming, pure freshening, pure warming, and pure freshening. Below $\gamma^n = 27.8$, the difference fields are not significant at the 90% confidence level and the R^2 value is not meaningful. Significantly, from the near surface to $\gamma^n = 27.6$ (below the salinity minimum) pure heave is not an important process for explaining the decadal differences.

2) THE SEASONAL DIFFERENCES

For the seasonal differences the pattern of variance explained by each process (Fig. 11b) contrasts strongly with the decadal differences. The rms noise in these data are similar to the decadal differences, but the amplitude of the differences are smaller. The near-surface waters between 190 and 500 db (γ^n between 26.69 and 26.95) are not well explained by either pure warming or pure heave. Although pure freshening does explain a higher percentage of variance, this process is noisy in this depth range. Between 500 and 1660 db (γ^n between 26.95 and 27.80) pure warming and pure freshening can be excluded except near two surfaces at neutral densities of 27.45 and 27.65. At $\gamma^n = 27.45$ pure warming is a statistically significant process, but is an artifact of the inversion: at this depth $\beta S'|_z$, $\beta S'|_n$, and $\mathcal{N}'\beta S_z$ change sign at the salinity minimum (Fig. 7c and 7d), where R_ρ is large (and changing rapidly as a function of depth). As a result, pure warming (defined by $\beta S'|_z = 0$) becomes significant in this small depth range: an unlikely result given that the change above and below this surface are characterized by heave. On the $\gamma^n = 27.65$ surface (at about 1360 db) pure freshening is also significant, although only slightly more so than heave. Because the significant freshening occurs only on two neutral surfaces, this process is excluded for the same reasons as the shallower surface described above. It appears that all of the seasonal differences in the main thermocline (regime II) can be explained by pure heave, and that pure warming and pure freshening processes associated with water mass changes are unimportant on this time scale.

6. Discussion

The results of the previous two sections for the seasonal and decadal differences are quite consistent with the time scales associated with ventilation of the Southern Ocean. On seasonal time scales, the mixed-layer region and part of the Sub-Antarctic Mode Water (SAMW, McCartney 1977) show water mass changes between the two *Franklin* repeat cruises (Fig. 9c). However, the changes are small in regime I, and although barely significant in the observations, the signs of $\theta'|_z$ and $\theta'|_n$ are both negative and plausibly consistent with negative heave (upwelling) and an increase of freshwater into near-surface and sub-antarctic mode water (SAMW) associated with this season. Below the SAMW the simplest interpretation of the observed seasonal differences is pure heave, moving neutral surfaces upward with no change in water mass properties ($\theta'|_n = S'|_n = 0$). Indeed, it would be surprising if either pure warming or pure freshening on seasonal time scales below 500 db were observed, since the mixing or advection of water masses from their source region has time scales of 10–100 years. The observed pure heave is probably the response of the thermocline in the Tasman Sea to local and nonlocal seasonal forcing.

On decadal time scales, advection and mixing of water masses from their source regions in the Southern Ocean can transport the effects of the changed surface conditions into the ocean interior. The observations show that the SAMW and the upper thermocline are

characterized mainly by warming (regime I, II, and III) with some freshening, causing significant cooling and freshening along neutral surfaces ($\alpha\theta'|_n < 0, \beta S'|_n < 0$), and a downward movement of these surfaces resulting in an increase of heat content. This broad interpretation is evident from Figs. 9a and 9b or Fig. 11a. The observations in Fig. 9a lie roughly along a single direction close to that of pure warming but with some influence of freshening, while in Fig. 9b where the pure warming process vector moves around through a range of angles, so do the observations, indicating that warming is more important than freshening. Our diagnosis of mainly pure warming is also consistent with other observations and supports the interpretation of these data by Bindoff and Church (1992). Analysis of surface air temperature data from ships and islands between 45° and 55°S suggests a warming of approximately 0.2°–0.4°C over the last three decades (Hansen and Lebedeff 1987, 1988; Jones 1988); it is in this range of latitudes where the SAMW and upper thermocline water is subducted and transported northward into the Tasman Sea across 43°S (Reid 1986).

The "pure freshening" in regime IV of the 23-year differences (Figs. 7b and 11a) is a surprising result. The data suggest that a freshening of sub-Antarctic frontal waters has occurred through increased precipitation or a changed interaction with sea ice. The changes in salinity on neutral surfaces at these depths are approximately 0.02 psu and are statistically significant at the 90% confidence level (Fig. 7b). The changes of this water, which outcrops on the southern flank of the Antarctic Circumpolar Current (~60°S), is consistent with the expected time scale for the northward transport of properties from this region. The change in the pattern of precipitation from observations over the Southern Ocean over the last 23 years is unknown. However, coupled ocean–atmosphere models for CO_2 doubling (Manabe et al. 1991) show an increase in precipitation over the Southern Ocean where these water masses outcrop. Our conclusion of surface freshening in this range of neutral densities seems quite robust because pure warming alone cannot be used to explain the observations. This conclusion provides some support for the numerical models.

The process approach that we have developed above for use with two snapshots of hydrographic data has important advantages over the traditional isopycnal analysis or the traditional comparison of data at constant depth. These advantages stem from explicitly recognizing three distinct ventilation processes of the thermocline and being able to objectively include each process in the interpretation of the observations, both at constant depth and measured along neutral surfaces.

The recent results of Roemmich (1992) of the warming of surface waters along the California coast could easily be interpreted in terms of the three subduction mechanisms. His results show significant trends in the temperature field with no change in salinity on isobars: the signature of our pure warming process. At Ocean Station Papa, Thomson and Tabata (1987) show that there have been significant changes of salinity and temperature both of which contribute to increases of steric sea level (our depth-integrated density anomaly), suggesting the presence of both positive pure freshening and warming.

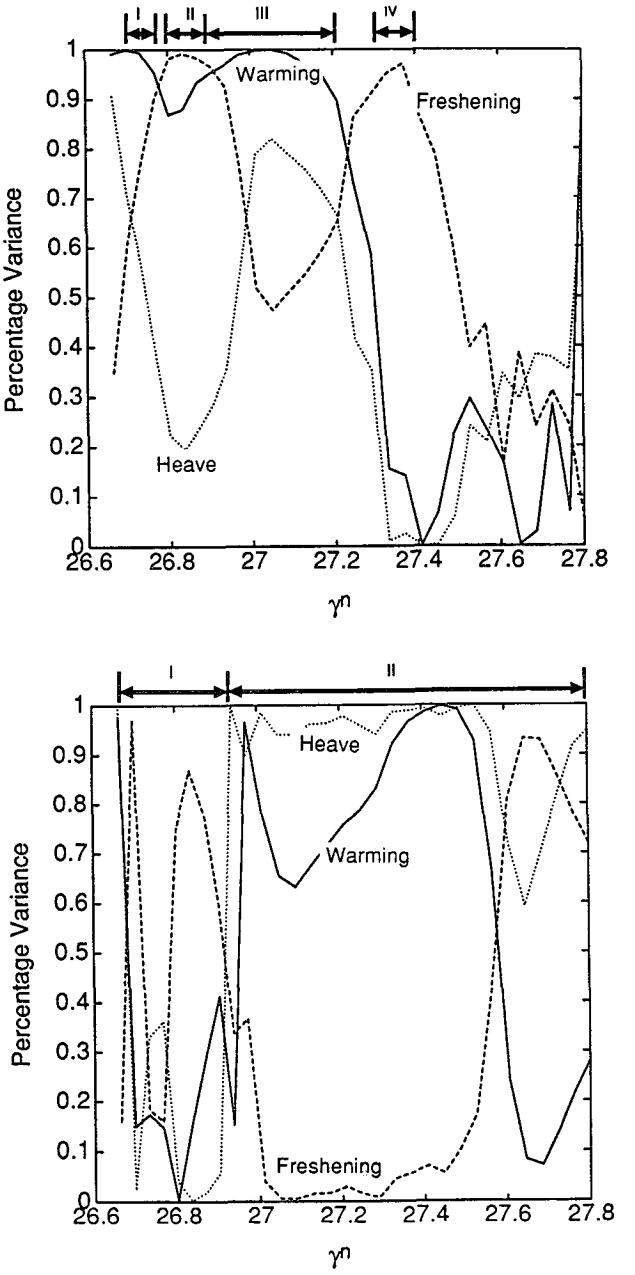

FIG. 11. The percentage variance explained for each process alone: (a) between the *Franklin* 1990 and SCORPIO data, and (b) between the 1990 and 1989 *Franklin* data. The continuous, dashed, and dotted lines are for pure warming, pure freshening, and pure heave, respectively.

For the 43°S data, it is remarkable that warming and freshening are the only processes that are significant over this 23-year period of the observations. That these two processes dominate is strong evidence that the statistically significant differences are caused by climatic variations associated with changes in surface forcing. Such changes in surface forcing could result from natural variations or from the enhanced greenhouse effect. The quite different role of warming and freshening compared with heave on decadal and seasonal time scales suggests that it may be possible to make the important distinction between temporal variations of hydrographic data caused by dynamical processes such as the generation and propagation of basin-scale waves and those of truly climatic origin.

Acknowledgments. We acknowledge the Australian Department of Environment, Sport, and Tourism (DEST) for the financial support that allowed the collection of the recent hydrographic data. Chief scientists Drs. J. Church and N. White and the master and crew of the RV *Franklin* are thanked for collecting excellent data on the *Franklin* and for making it available to us. We thank Dr. D. R. Jackett for labeling the data with the neutral density variable.

REFERENCES

Bendat, J. S., and A. G. Piersol, 1986: *Random Data: Analysis and Measurement Procedures.* John Wiley and Sons, 566 pp.

Bindoff, N. L., and J. A. Church, 1992: Warming of the water column in the south-west Pacific. *Nature,* **357,** 59–62.

Church, J. A., J. S. Godfrey, D. R. Jackett, and T. J. McDougall, 1991: A model of sea level rise caused by ocean thermal expansion. *J. Climate,* **4,** 438–456.

Hansen, J., and S. Lebedeff, 1987: Global trends of measured surface air temperature. *J. Geophys. Res.,* **92,** 13 345–13 372.

——, and ——, 1988: Global surface air temperatures: update through 1987. *J. Geophys. Res. Lett.,* **15,** 323–326.

Iselin, C. O'D., 1939: The influence of vertical and lateral turbulence on the characteristics of the waters at middepths. *Eos, Trans. Amer. Geophys. Union,* **20,** 414–417.

Jackett, D. R., and T. J. McDougall, 1994: On the labelling of hydrographic data with neutral density.

Jones, P. D., 1988: Hemispheric surface air temperature variations: Recent trends and an update to 1987. *J. Climate,* **1,** 654–660.

Manabe, S., K. Bryan, and M. J. Spelman, 1990: Transient response of a global ocean–atmosphere model to a doubling of atmospheric carbon dioxide. *J. Phys. Oceanogr.,* **20,** 722–749.

——, R. J. Stouffer, M. J. Spelman, and K. Bryan, 1991: Transient response of a coupled ocean–atmosphere model to gradual changes of atmospheric CO_2. Part I: Annual mean response. *J. Climate,* **4,** 785–818.

McCartney, M. S., 1977: Subantarctic mode water. *A Voyage of Discovery,* M. Angel, Ed., Pergamon Press, 696 pp.

McDougall, T. J., 1987: Neutral surfaces. *J. Phys. Oceanogr.,* **17,** 1950–1964.

——, and Y. You, 1990: Implications of the nonlinear equation of state for upwelling in the ocean interior. *J. Geophys. Res.,* **95,** 13 263–13 276.

Menke, W., 1984: *Geophysical Data Analysis: Discrete Inverse Theory.* Academic Press, 260 pp.

Nurser, A. J. G., and J. C. Marshall, 1991: On the relationship between subduction rates and diabatic forcing of the mixed layer. *J. Phys. Oceanogr.,* **21,** 1793–1802.

Pedlosky, J., and P. Robbins, 1991: The role of finite mixed-layer thickness in the structure of the ventilated thermocline. *J. Phys. Oceanogr.,* **21,** 1018–1031.

Pollard, R. T., and S. Pu, 1985: Structure and circulation of the upper Atlantic Ocean northeast of the Azores. Vol. 14, *Progress in Oceanography,* Pergamon, 443–462.

Reid, J. L., 1986: On the total geostrophic circulation of the South Pacific Ocean: Flow patterns, tracers and transports. Vol. 16, *Progress in Oceanography,* Pergamon, 1–61.

Roemmich, D., 1983: Optimal estimation of hydrographic station data and derived fields. *J. Phys. Oceanogr.,* **13,** 1544–1549.

——, 1992: Ocean warming and sea-level rise along the southwest U.S. coast. *Science,* **257,** 373–375.

Speer, K., and E. Tziperman, 1992: Rates of water mass formation in the North Atlantic Ocean. *J. Phys. Oceanogr.,* **22,** 93–104.

Stommel, H., 1979: Determination of water mass properties of water pumped down from the Ekman layer to the geostrophic flow below. *Proc. Natl. Acad. Sci. USA,* **76,** 3051–3055.

——, E. D. Stroup, J. L. Reid, and B. Warren, 1973: Transpacific hydrographic sections at Lats. 43°S and 28°S: The SCORPIO Expedition—1. Preface. *Deep-Sea Res.,* **20,** 1–7.

Thomson, R. E., and S. Tabata, 1987: Steric height trends at Ocean Station Papa in the northeast Pacific Ocean. *Mar. Geod.,* **11,** 103–113.

Tziperman, E., 1986: On the role of interior mixing and air–sea fluxes in determining the stratification and circulation of the oceans. *J. Phys. Oceanogr.,* **16,** 680–693.

Walin, G., 1982: On the relation between sea-surface heat flow and thermal circulation in the ocean. *Tellus,* **34,** 187–195.

Warren, B. A., 1973: Transpacific hydrographic sections at Lats. 43S and 28S: The SCORPIO expedition—II. Deep water. *Deep-Sea Res.,* **20,** 9–38.

Woods, J. D., 1985: The physics of thermocline ventilation. *Coupled Atmosphere–Ocean Models,* J. C. J. Nihoul, Ed., Elsevier, 767 pp.

Wunsch, C., D. Hu, and B. Grant, 1983: Mass, heat, salt, and nutrient fluxes in the South Pacific Ocean. *J. Phys. Oceanogr.,* **13,** 725–753.